

# Multiscale crustal architecture of Alaska inferred from P receiver functions

Meghan S. Miller<sup>1,\*</sup>, Leland J. O'Driscoll<sup>2</sup>, Robert W. Porritt<sup>3</sup>, and Sarah M. Roeske<sup>4</sup>

<sup>1</sup>RESEARCH SCHOOL OF EARTH SCIENCES, AUSTRALIAN NATIONAL UNIVERSITY, BUILDING 142, MILLS ROAD, CANBERRA, ACT 2601 AUSTRALIA

<sup>2</sup>DEPARTMENT OF EARTH SCIENCES, UNIVERSITY OF OREGON, 100 CASCADE HALL, 1275 E 13TH AVENUE, EUGENE, OREGON 97403, USA

<sup>3</sup>INSTITUTE FOR GEOPHYSICS, JACKSON SCHOOL OF GEOSCIENCES, UNIVERSITY OF TEXAS, AUSTIN, 2305 SPEEDWAY STOP C1160, AUSTIN, TEXAS 78712-1692, USA

<sup>4</sup>DEPARTMENT OF EARTH AND PHYSICAL SCIENCES, UNIVERSITY OF CALIFORNIA, DAVIS, ONE SHIELDS AVENUE, DAVIS, CALIFORNIA 95616, USA

## ABSTRACT

The geologic mosaic of continental and oceanic terranes, displaced and deformed by multiple plate reorganization episodes, rapid lateral topographic variations, and heterogeneous distribution of strain throughout Alaska, all predict strong variability of crustal architecture. We present the first wide-scale model of crustal thickness based on broadband seismic data across the region that is constrained where seismic instrumentation has been deployed; dense coverage in the south-central region and more sparse coverage in the western and Arctic regions as the USArray Transportable Array (TA) is installed. Analyses of P receiver functions (PRFs) provide the first detailed look at crustal structure across all of Alaska. The variable thickness reflects inherited structure from Mesozoic to early Cenozoic convergent and extension events that in some regions is being extensively modified by ongoing convergence and collision, particularly along the active southern margin.

Beneath the southern Alaska forearc to the central Alaska Range, the Yakutat slab Moho is also observed, illustrating the most recent ongoing accretionary event resulting from the collision of the Yakutat microplate. Combining three different receiver function methodologies, i.e., common conversion point stacking, receiver function stacks, and receiver gathers, for viewing and imaging P receiver functions allows for an interpretation of Alaskan crustal structure that spans multiple scales. The four-dimensional interpretation of the Alaskan crust will continue to evolve as the full TA is deployed and geologic studies are combined with the interpretations from this extensive seismic experiment.

LITHOSPHERE, v. 10; no. 2; p. 267–278; GSA Data Repository Item 2018070 | Published online 30 January 2018

<https://doi.org/10.1130/L701.1>


## INTRODUCTION

The northern Cordillera contains an amalgamation of terranes that have undergone multiple episodes of displacement due to plate boundary reorganization, strike-slip translation, and convergent margin induced orogenesis (Plafker and Berg, 1994). The distinction between terranes is based on crustal type, paleogeographic origin, and tectonic history, and some of them in northern and western Alaska contain Proterozoic basement and multiple orogenic events. Most of the Alaskan crust was formed during the Phanerozoic with final assembly of the terranes in northern and central Alaska occurring primarily in the late Mesozoic along the Laurentian margin. From around Fairbanks, to the south and in western Alaska, crustal features continue to be modified in the Cenozoic, with possible localized thinning in the interior and western Alaska, and continued tectonic accretion and episodic arc activity along the Pacific–North America plate boundary in the south. This southern margin displays remarkable along-strike variation (Fig. 1A). Arc-producing subduction below the Aleutian Islands exhibits a moderate subduction angle with strain focused at the plate interface (Cross and Freymueller, 2008), and transitions eastward to an amagmatic section (McNamara and Pasyanos, 2002; Rondenay et al., 2010; Finzel et al., 2011) that coincides with ongoing shallow angle subduction and large-magnitude convergence (e.g., Pavlis et al., 2012). The subduction, collision, and translation of the Yakutat terrane, a thick

section of mafic crust, is the ongoing and most recent exotic terrane collision with the North American continent.

Seismic imaging from tomography, receiver functions, and active source experiments have previously been used as tools to investigate the crustal velocity structure of Alaska and the Northern Cordillera and therefore their tectonic history. Due to the limited data available prior to the late 1990s and early 2000s, the resolution of the known structure of the mantle and lithosphere is highly variable and in some places quite poor, especially in the Alaskan interior and on the margins of the important transition between subduction of the Pacific oceanic lithosphere and collision of the Yakutat plateau. The TACT (Trans-Alaskan Crustal Transect) active source experiment (Fuis et al., 2008, and references within) provided images of the complexity of the crust in the first seismic transect across Alaska. This series of papers on the TACT experiment identified the thickest crust and distinctive crustal structure characteristics beneath the highest topography at the north (Brooks Range) and south ends of the transect (Pacific margin) (Fuis et al., 2008). More recent onshore-offshore active seismic experiments (such as the St. Elias Erosion and Tectonics Project, STEEP; Worthington et al., 2012; Christeson et al., 2013) have effectively imaged and tracked the Yakutat plateau offshore through the forearc.

Broadband seismic imaging results have primarily been concentrated along a series of linear or small aperture arrays, mostly in south-central Alaska, that have imaged the crust and uppermost mantle. These studies have focused on the Yakutat terrane (e.g., Kim et al., 2014; Bauer et al., 2014) and subduction zone structure northward below the Alaska Range and Denali fault (e.g., Ferris et al., 2003; Eberhart-Phillips et al., 2006;

Meghan Miller  <http://orcid.org/0000-0001-5494-2296>

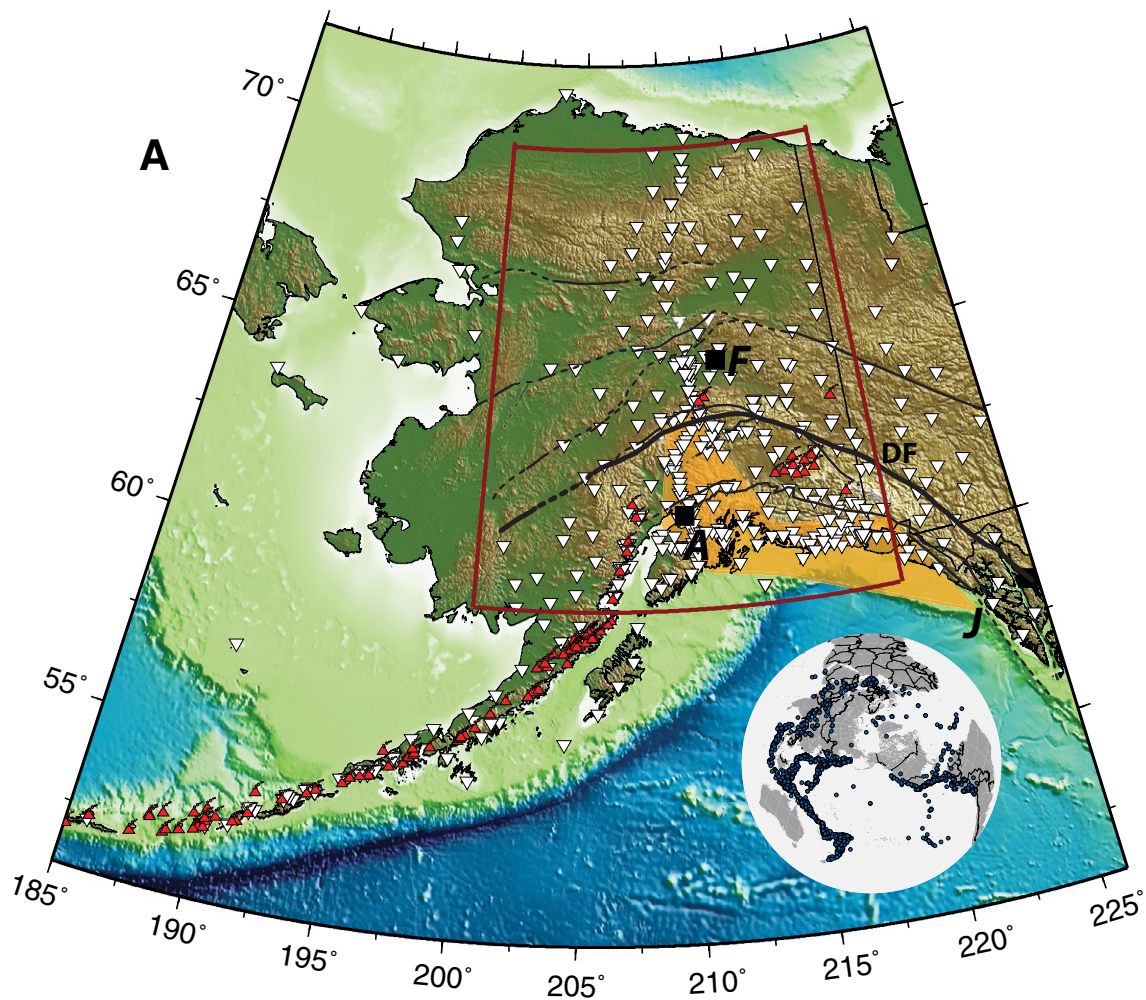


Figure 1 (Continued on following page).

Rondenay et al., 2010; Brennan et al., 2011; Wang and Tape, 2014), illustrating sharp structures, such as the low-velocity zone on top of the slab, and possible steps in the crust-mantle boundary at fine (few kilometers) resolution. These works have illustrated the active collision and accretion of the Yakutat microplate onto and beneath the North American plate. In particular, Wang and Tape (2014) produced a 3D isotropic velocity model and anisotropy phase velocity maps from teleseismic Rayleigh wave analysis to infer the dominance of the Yakutat terrane influence on flow patterns and the structure of the crust and uppermost mantle. Brennan et al. (2011) imaged the crustal structure further inland across the Alaska Range with P receiver functions (PRFs) and used P-wave tomography from Eberhart-Phillips et al. (2006) to interpret the suture between the continental margin and the allochthonous Wrangellia oceanic terrane that is south of the Denali fault. These results suggest that older collisional events (1) are a fundamental mechanism for growing the continents, (2) are preserved in the crustal structure, and (3) can be detected with broadband seismic imaging. More recent S receiver functions (SRFs) by O'Driscoll and Miller (2015), using all available data at the time, further advocated that observed changes in lithospheric thickness across Alaska are also linked to the geologically defined tectonic domains and to the response of the lithosphere to the active collision of the Yakutat, albeit with more coarse resolution than work presented herein.

Here PRFs are used to map the crustal structure across Alaska and relate the imaged structure to the tectonic history of terranes that have created and formed the Northern Cordillera portion of the North American lithosphere. The data analyzed include the EarthScope Transportable Array (TA) and all other existing broadband data from 1999 through April 2017 that provide the first state-wide analysis of the crust that improves the understanding of the long-term tectonic history of the region.

#### DATA AND METHODS

PRFs were calculated using an upgraded version of FuncLab (Eagar and Fouch, 2012; Porritt and Miller, 2018) where the waveform data were retrieved within FuncLab through use of the `irisFetch.m` MATLAB script (Trabant et al., 2012). Earthquakes with magnitudes  $>M6.0$  at epicentral distances between  $30^\circ$  and  $98^\circ$  were used as sources for the analysis. We utilize multiple networks (see Data Repository Table DR1<sup>1</sup> for DOI numbers

<sup>1</sup>GSA Data Repository Item 2018070, Table DR1: Seismic networks with DOIs; Table DR2: Moho depth estimates at station locations; Figure DR1: receiver gathers at 3 stations; Figure DR2: CCP volume profiles and hit count; Figure DR3: 3D ray diagram of receiver functions at AK.WAT2; and Figure DR4: receiver function record sections sorted by backazimuth at two stations, is available at <http://www.geosociety.org/datarepository/2018>, or on request from [editing@geosociety.org](mailto:editing@geosociety.org).

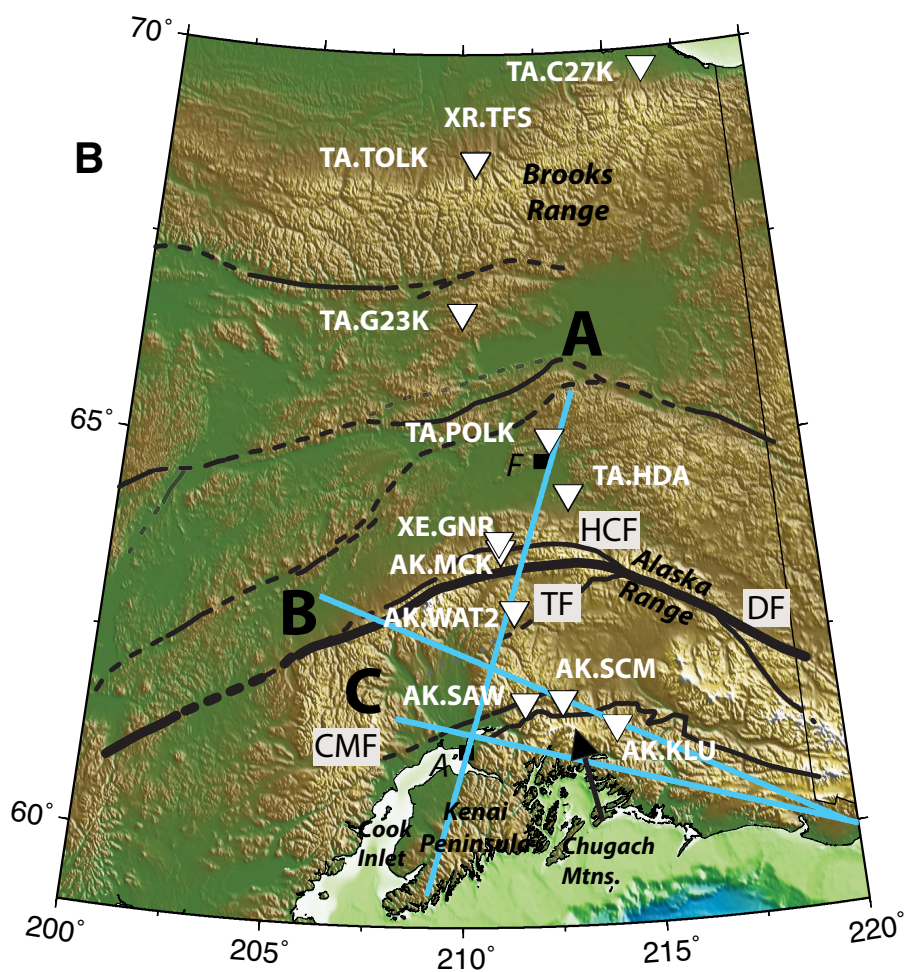


**Figure 1.** Map of the broadband seismic stations used in the P receiver function (PRF) analysis (white inverted triangles), including active volcanoes (red triangles; Smithsonian Global Volcanism Program), major faults (shown with black or gray lines; dashed where approximately located; gray indicates located by magnetic gradients in part), the Denali fault (DF; shown with the thickest black line). (A) Map of all the stations analyzed; the interpreted location of the Yakutat terrane from Fuis et al. (2008) is shown with an orange-shaded polygon, and red polygon indicates the location of the map in B. Black squares with letters in italics indicate cities: F—Fairbanks, A—Anchorage, J—Juneau. Globe inset shows map of the earthquakes (blue dots) analyzed. (B) Map of the locations of the cross sections in Figure 2 indicated by cyan lines and the location of the stations presented in Figure 3 and Figure DR2. HCF—Hines Creek fault; TF—Talkeetna fault; CMF—Castle Mountain fault.

for each of the networks) hosted at the IRIS (Incorporated Research Institutions for Seismology) Data Management Center (Fig. 1). A total of 2094 events (Fig. 1 inset) and 468 stations yielded 117,079 preliminary PRFs that were manually edited and picked with the FuncLab trace editor based on appearance of high signal-to-noise direct arrivals for a final 24,188 receiver functions. Iterative time-domain deconvolution (Ligorria and Ammon, 1999) of the vertical component from the radial and transverse components was performed about a 1 Hz central frequency. This central frequency was chosen due to the relatively large amount of energy at 1 Hz on teleseismic P arrivals and sensitivity to crustal-scale features. This also affects the lateral sensitivity in the Fresnel zone when the P to S conversions are spatially mapped.

We use multiple techniques to visualize and analyze the receiver functions due to the variable spacing of the seismic stations across Alaska. Individual receiver functions at each station can be stacked with a simple summation to suppress noise, improve the signal-to-noise ratio, and emphasize coherent conversions. The receiver gather stacks are migrated to depth (from time) using the one-dimensional (1D) velocity model *ak135* (Kennett et al., 1995) to provide an estimate of the average structure at depth beneath each station. Individual receiver functions (one event at one station) provide spot measurements at points along raypaths at depth some distance away from the station. They are used to analyze the variation in signal by backazimuth, and therefore provide more information than the average immediately below the station. We also compute a 3D model of the upper mantle discontinuities via common conversion point (CCP)

stacking (e.g., Dueker and Sheehan, 1997), which repositions energy from the converted phases in the subsurface beneath the station by implementing depth mapping and accounting for Fresnel zone effects along the ray path. The receiver functions are migrated to depth using the 3D velocity model GyPSuM (Simmons et al., 2010). The width of sensitivity of the receiver function along the ray path is determined by the Gaussian width used in the receiver functions (2.5) and the velocity in the 1D model. The amplitudes are then stacked into nonoverlapping spatial bins of size  $0.5^\circ \times 0.5^\circ$  by 1 km, spanning lat  $52^\circ\text{N}$  to  $71^\circ\text{N}$ , long  $135^\circ\text{E}$  to  $174^\circ\text{E}$ , and 0 to 160 km depth, providing resolution of a few kilometers in depth. Only regions that are well covered by stations can be considered resolved, and therefore our discussion focuses on those areas.

## RESULTS AND INTERPRETATIONS

### Common Conversion Point Stacking

The station density in southern and central Alaska was sufficient (Fig. 1) to produce a Common Conversion Point (CCP) stacked receiver function volume. A series of vertical cross sections many hundreds of kilometers long through the volume show the large-scale differences in crustal thicknesses and crustal architecture (Fig. 2). Distinct changes in crustal and uppermost mantle structure as inferred from the CCP stacked receiver function images are observed both across and within terranes,



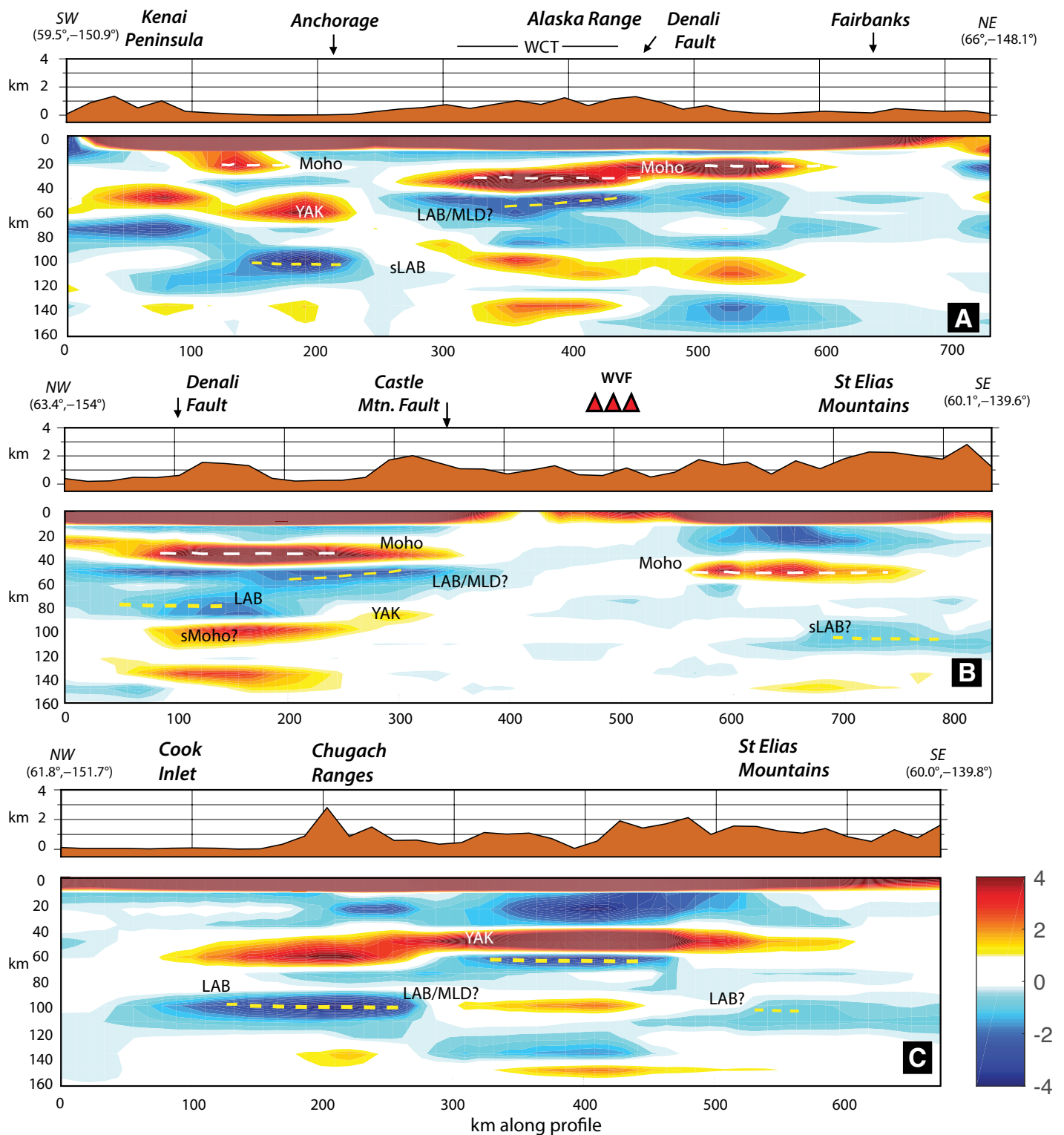


**Figure 2.** Cross sections through the common conversion point volume along the profiles as indicated in Figures 1B and 4. Topography is plotted at the top of each cross section for reference along with geologic features. The positive red signals indicate seismically fast-to-slow conversions (e.g., Moho), and negative blue signals indicate slow-to-fast conversion (e.g., lithosphere-asthenosphere boundary, LAB). (A) North-south cross section from the Kenai Peninsula inland to north of Fairbanks. WCT—Wrangellia composite terrane (terrane boundaries are shown in Fig. 4); YAK—Yakutat terrane at depth; MLD—mid-lithosphere discontinuity. (B) Northwest-southeast cross section that is south of the Wrangell Volcanic Field (WVF). (C) Northwest-southeast cross section through the Yakutat terrane. The interpreted locations of the Moho are indicated by white dashed lines and the inferred depth to the LAB is marked with yellow dashed lines.

which requires combining geologic observations and constraints in order to interpret the significance of the geophysical signal. In the CCP profiles (Fig. 2), positive red signals indicate seismically fast-to-slow conversions (e.g., Moho), and negative blue signals indicate slow-to-fast conversion (e.g., lithosphere-asthenosphere boundary). The profiles are annotated with interpretations of these conversions and the expected complex velocity change interface structure in the crust and uppermost mantle.

### Central Alaska

The north-south profile through the CCP volume (Fig. 2A), from the Kenai Peninsula to north of Fairbanks, captures a cross-sectional view of the crust and uppermost mantle from the active convergent margin to the relatively stable interior. There are abrupt changes in apparent positive conversion signals at Moho depths (~30–45 km), particularly in the southern portion of the profile into central Alaska (Wrangellia composite terrane, WCT) and across the Denali fault system. At the northern extent of the profile (>600 km) the signal becomes weak because there are fewer stations to contribute to the image, but it suggests that there is a more simple structure north of the Denali fault.

### Yakutat Microplate

In the north-south profile (Fig. 2A) there are multiple conversions at depths >40 km in the first ~250 km of the profile. The positive conversion at ~45–60 km is inferred to be from the subducted Yakutat microplate and the deeper negative conversion may be the base of the subducted slab. In contrast to the complexity observed in the north-south profile, the northwest-southeast profile, shown in Figure 2B, inboard of the northern extent of the inferred Yakutat microplate on the southeastern end (Fig. 1), is relatively simple. This section illustrates the crustal and lithospheric structure where the plate boundary transitions from the convergent margin in the west into primarily transverse motion to the east. The Moho is shallower beneath the northwest portion of the profile and is deeper beneath the southeastern segment of the profile (Fig. 2B). The northwestern end of the cross-section also has multiple positive and negative deep (below the Moho) conversion signals, with possible signals from the subducted slab and subducted or underthrust Yakutat microplate.

Figure 2C is a cross section that traverses entirely through the inferred Yakutat microplate (Fig. 1). The structure indicated from the interface conversions appears to be the simplest of the three profiles, yet is a vertical cross section through a tectonically complex and active plate margin. In this profile, one of the highest amplitude positive signals is at a depth between ~50 and 65 km, but there are no shallower positive amplitude signals. The deeper (~105 km) negative amplitude on the northwestern segment (between 50 and 275 km distance) is inferred to be the lithosphere-asthenosphere boundary and in the middle of profile, beneath the Chugach, there is a shallower (~65 km) negative signal.

The CCP images illustrate large-scale variations in lithospheric structure, but the details beneath each terrane and/or station are smoothed out or perhaps even missing due to the imaging technique. In addition, the CCP volume does not cover the entire state because of the widely dispersed and irregular density of seismometers at this time across the majority of Alaska. Therefore, additional insight is found from more detailed analysis of data at individual stations.

### Receiver Function Stacks

For each stack, the 1D, depth-mapped, individual receiver functions are summed to create a single PRF as a function of depth (Fig. 3). This provides a simple picture of structure under the station, but at the cost of losing information from possible backazimuthal variation. Furthermore,

because this method uses a 1D velocity model, there is an additional ~1–2 km depth uncertainty due to variations from the actual velocity structure. Nonetheless, the terrane-wide differences in Moho depth observed are greater than the uncertainty that could be due to the stacking process. For the remote northern and western portions of Alaska, there are only sparsely located stations, and the individual stations are critical.

Overall, the station stacked receiver gathers indicate significant variation between different terranes (Fig. 4). In a broad sense, the crustal thickness north of the Alaska Range generally matches the local topography, where the deepest Moho is located beneath the high topography and the shallowest Moho is located beneath lower topography, but with some interesting exceptions.

### Northern Alaska

The stacked receiver functions for stations TA.TOLK and XR.TFS (Fig. 3A; Fig. DR1) in the Brooks Range of northern Alaska (locations shown in Figs. 1B and 4) indicate a relatively simple crustal structure with a relatively thick crust (~48 km). The thick crust (~45 km) appears to continue eastward to the most northeastern station in Alaska, TA.C27A (Fig. 3B; location in Figs. 1B and 4). Southwest of the Brooks Range, in the Ruby terrane, the crust is notably thinner (~35 km), as shown by the receiver gather stack for station TA.G23K (Fig. 3C; location in Figs. 1B and 4). Although the tectonic history of the Ruby terrane is significantly different from that of interior Alaska, the crustal thickness is comparable, as seen at stations TA.POKR and AK.HDA (locations shown in Figs. 1B and 4), near Fairbanks (Figs. 3D, 3E). The crust beneath TA.POKR (Fig. 3D) is ~33 km thick, which is within the Yukon Tanana terrane (YTT) north of Fairbanks (Figs. 1B and 4). Farther south but still within the YTT, in the Tanana Valley, station AK.HDA (Fig. 3E) indicates the Moho is at ~29 km depth.

### Central Alaska

In the Alaska Range north of the Denali fault system (locations shown in Figs. 1B and 5), the stacked receiver functions at XE.GNR (Fig. 3F) indicate that the Moho depth is comparable (~33 km) to that beneath the YTT terrane (Fig. 3D). However, within the Alaska Range suture zone at stations AK.MCK and AK.WAT2 (Figs. 3G, 3H) the Moho depth is considerably deeper (~40 km), which was also apparent in the CCP profile (Fig. 2A). Through investigating the receiver functions at individual stations, rather than just the CCP profile, we find that the significant change in thickness actually occurs across the Hines Creek fault, which is on the northern flank of the high topography of the Alaska Range. The ~8 km offset is illustrated by two stations on either side of the fault, AK.MCK to the south and XE.GNR to the north (Figs. 3G, 3F).

### Yakutat Microplate

Further south within central Alaska, the stations that are above the inferred position of the Yakutat at depth (Fig. 1A) and within the active convergent margin indicate a very deep Moho and complicated crustal structure. Figures 3I and 3J illustrate two representative receiver function gathers from stations in the west-central Chugach Mountains (see locations in Figs. 1B and 5), which appear to have very different structures although they are in a similar terrane and located close to one another. Station AK.SAW has a positive signal at ~31 km depth, but it also has a lower amplitude positive signal at ~60 km. In contrast, station AK.SCM only has one large-amplitude positive signal at ~60 km depth, similar to station AK.KLU farther to the east (Fig. DR1C; see Fig. 4 for station location).

### Kodiak Island and Alaska Peninsula

The island stations and stations near the coast can be highly variable in data quality, but the stack receiver functions (Figs. 3K, 3L) for two long

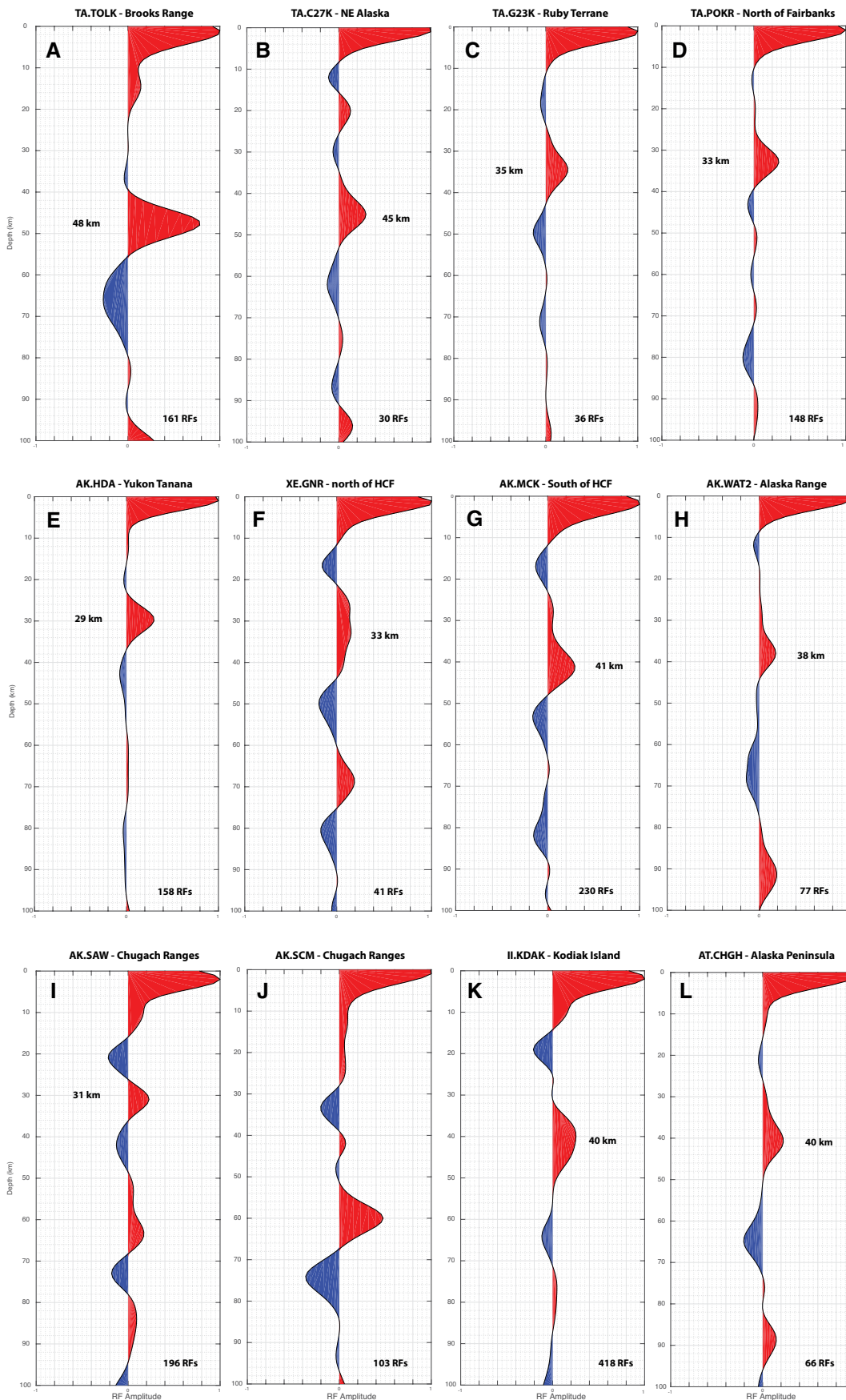


**Figure 3. Receiver gathers for 8 stations with locations indicated in Figures 1B, 4, and 5. The first positive amplitude signal (in red) at depth is interpreted to be the Moho signal, with the depth (in km) indicated in each panel as picked within the FunLab (see Porritt and Miller, 2018) picking routine. The number of receiver functions (RF) used to create the gather is listed in the bottom right of each panel.**

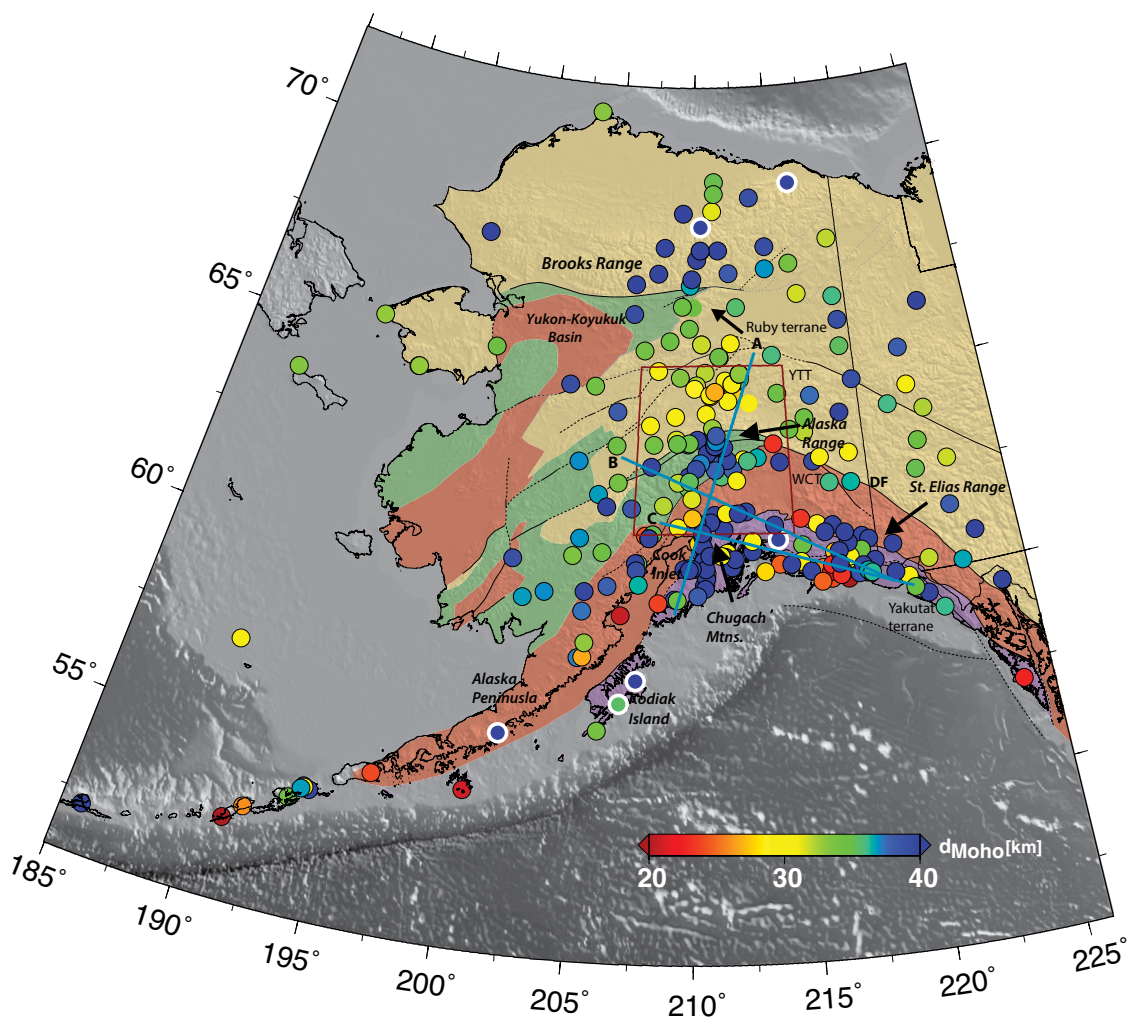


**Figure 4.** Moho depth ( $d$ ) estimates at station locations with more than 15 receiver functions overlain by major faults in thin black and gray lines (dashed where approximately located; gray indicates located by magnetic gradients in part). Map colors denote broad crustal categories of terranes, based primarily on dominant bedrock geology and isotopic characteristics: yellow—continental and marginal basins, including Yukon-Tanana terrane (YTT); orange-red—ocean plateau and arc, including the Wrangellia composite terrane (WCT); green—clastic marine basins; purple—accretionary complex. The circles with white outlines are stations discussed in detail in the text and shown in Figure 3 (Fig. DR1). From north to south: TA.C27K, northeastern Alaska; TA.TOLK and XR.TFS, northern stations in the Brooks Range; AK.KLU, in the Chugach Mountains; IL.KDAK, at the eastern end of Kodiak Island; AT.OHAK, in central Kodiak Island; AT.CHGH, on the Alaska Peninsula. The red polygon denotes the area presented in Figure 5. DF—Denali fault.

running stations on Kodiak Island (locations shown in Fig. 4), IL.KDAK and AT.OHAK, indicate that the crustal thickness are  $\sim 40$  and  $\sim 36$  km, respectively. Station AT.CHGH on the Alaska Peninsula (location in Fig. 4) also has a Moho conversion indicating another relatively deep Moho at  $\sim 40$  km depth (Fig. 3L).

### Moho Depth Map

To assess the crustal thickness across Alaska using all the available data from the broadband stations (Fig. 1A), we produced a Moho depth map based upon the receiver function stacks. The depth to the Moho was hand-picked for all stations within FuncLab (Porritt and Miller, 2018), then the picks for stations that had more than 15 receiver functions were used to produce a Moho depth map (Figs. 4 and 5). Although there are

some areas with limited data and some with very complex signals, the map indicates a primary trend that the crustal thickness roughly correlates with topography: (1) thick crust beneath the Brooks Range and northern Alaska; (2) thinner crust in the YTT in central Alaska; (3) thick crust beneath the Alaska Range. However, the cause of complex heterogeneous crustal structure in southern Alaska, including the arc, is not nearly as clear.

For the stations along the coast, through the volcanic arc, and above the Yakutat terrane there is significant variability in Moho depth and crustal structure. This has been documented previously (e.g., Bauer et al., 2014; Ward, 2015). For example, Bauer et al. (2014) argued that the geometry of the crust-mantle boundary structure varies systematically from west to east. The Moho thickness map generally supports their interpretation; however, the variations shown in Figure 4 are not systematically linked to the convergent plate boundary changes.



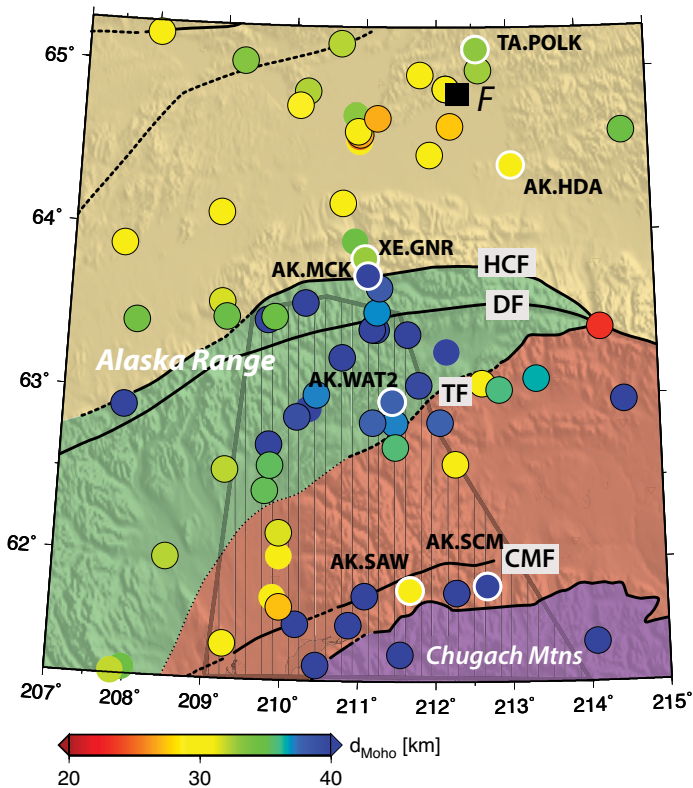


**Figure 5.** Moho depth ( $d$ ) estimates at stations located in central Alaska with more than 15 receiver functions. See Figure 4 for terrane descriptions. The black lines indicate major faults; solid are well located, dashed are buried, dotted are inferred from magnetic anomalies combined with regional-scale geologic maps. HCF—Hines Creek fault; DF—Denali fault; TF—Talkeetna fault; CMF—Castle Mountain fault. The polygon with a lined pattern represents the interpreted extent of the Yakutat terrane at depth from Fuis et al. (2008). The circles with white outlines are stations that are discussed in the text and in Figure 3. These stations are also highlighted in Figure 1B. From north to south: TA.POLK—station north of Fairbanks; TA.G23K—southern station in the Ruby terrane; AK.HDA—central Alaska station south of Fairbanks; XE.GNR—station north of HCF; AK.MCK—station south of HCF; AK.WAT2—station in the Alaska Range north of Talkeetna fault; AK.SAW and AK.SCM—stations in the Chugach Mountains. The black square labeled F indicates Fairbanks.

### Receiver Function Gathers

The receiver function stacks provide a glimpse of the average structure below each station, but the individual receiver functions at each station can be plotted as gathers in order to evaluate more detailed structure beneath the station that may be lost when all the receiver functions are summed into one trace. The gathers (Figs. 6 and 7) contain all the individual receiver functions at a station, plotted either by backazimuthal variation or ray parameter.

The station stacks (Fig. 3H), station AK.WAT2 in the Alaska Range suture zone, indicate a fairly thick crust (~38 km) that is also observed throughout the suture zone (location shown in Figs. 1B and 5). This 38 km depth signal, interpreted as the Moho, is also apparent in the receiver gathers at ~4.5 s (Fig. 6). The black line is the predicted arrival time (P37s) for a Moho conversion at 37 km depth. The receiver gathers, however, accentuate a large-amplitude positive signal at ~10 s (Fig. 6). This is apparent when the gathers are sorted by ray parameter (lateral moveout) as in Figure

6A, but is more striking when they are sorted by event backazimuth (Fig. 6B). This signal at ~10 s is only observed from earthquakes originating from ~230°–315° backazimuth range (Fig. 6B). Figure DR3 illustrates the raypaths in depth converted space (assuming the 1D velocity model ak135; Kennett et al., 1995). This view shows that the high-amplitude positive conversion is at a consistent depth for multiple PRFs with varying incidence angles. These gathers, and specifically analyzing individual receiver functions by backazimuth and ray parameter, suggest that the later positive signal at 10 s is a conversion at ~90 km depth. This arrives too early and too deep for a crustal multiple (P37pPs), as shown by the dotted lines in Figure 6A, and the amplitude of the signal is too large for a multiple; therefore, we infer this to be a conversion from the leading edge of the subducted Yakutat terrane. The inferred mapped position of the Yakutat (Fuis et al., 2008; Eberhart-Phillips et al., 2006) in Figures 1 and 5 shows that station WAT2 is just above its downdip extent.

Further south, toward the shallower portion of the Yakutat subducted slab, the receiver function gathers show complexity owing to the active collision, which is mostly hidden in the CCP profiles. The signal from the Moho appears to be unusually deep from both the CCP profiles (Fig. 2C) and the receiver function stacks (Figs. 3I, 3J). Receiver gathers for two stations in the Chugach mountains northern range front (shown in Figs. 7A, 7B), are only ~50 km away from each other, but the signals show sharp contrast. Station AK.SAW (Fig. 7A) shows a clear Moho signal at ~32 km depth (~3.5 s) and an internal crustal positive signal. In contrast, station AK.SCM (Fig. 7B) appears to only have a large-amplitude positive pulse at ~7 s and lacks a Moho signal from most azimuths or ray parameters. Figure DR4 shows the receiver gathers for AK.SAW and AK.SCM sorted by backazimuth, where AK.SCM has a weak signal from the west-southwest (225°–270°) at 3.5 s that may be from a shallow Moho, but overall this lack of signal in the individual receiver functions results in the apparent lack of Moho in the CCP stacked images (Fig. 2C).

### DISCUSSION

The analysis of receiver functions for the ~470 stations deployed across Alaska provides an overview of the wide range of crustal thickness and architecture across this vast area. Profiles through the CCP volume provide images of the largest scale structure in the most densely instrumented part of central and southern Alaska. Additional analysis of station stacks and receiver function gathers provides information about not only the isolated stations in the north and west, for example, but also important detailed information about the structure beneath and around each station where CCP imaging can smooth out or obscure finer scale crustal structure. Combining all of the various visualizations with geological constraints provides fundamental observations on crustal and upper mantle architecture that reflect the tectonic history of Alaska.

### Northern Alaska

The observed thick crust, from the Moho depth map and the receiver function gathers, beneath the Brooks Range is in agreement with the TACT line (Fuis et al., 2008) interpretations and potential field analysis (e.g., Saltus and Hudson, 2007). The range formed in the mid-late Mesozoic as an arc-continental block collision that resulted in hundreds of kilometers of crustal shortening, as exhibited by large-scale crustal duplexes. The relatively thick crust beneath the Yukon-Koyukuk basin is more of a surprise, as the region is topographically very low (<100 m), and although parts of this Mesozoic marine sedimentary and volcanic basin contain isoclinal folding, no large-scale crustal shortening has been documented in the basin (Patton and Box, 1989). The juxtaposition across the terrane



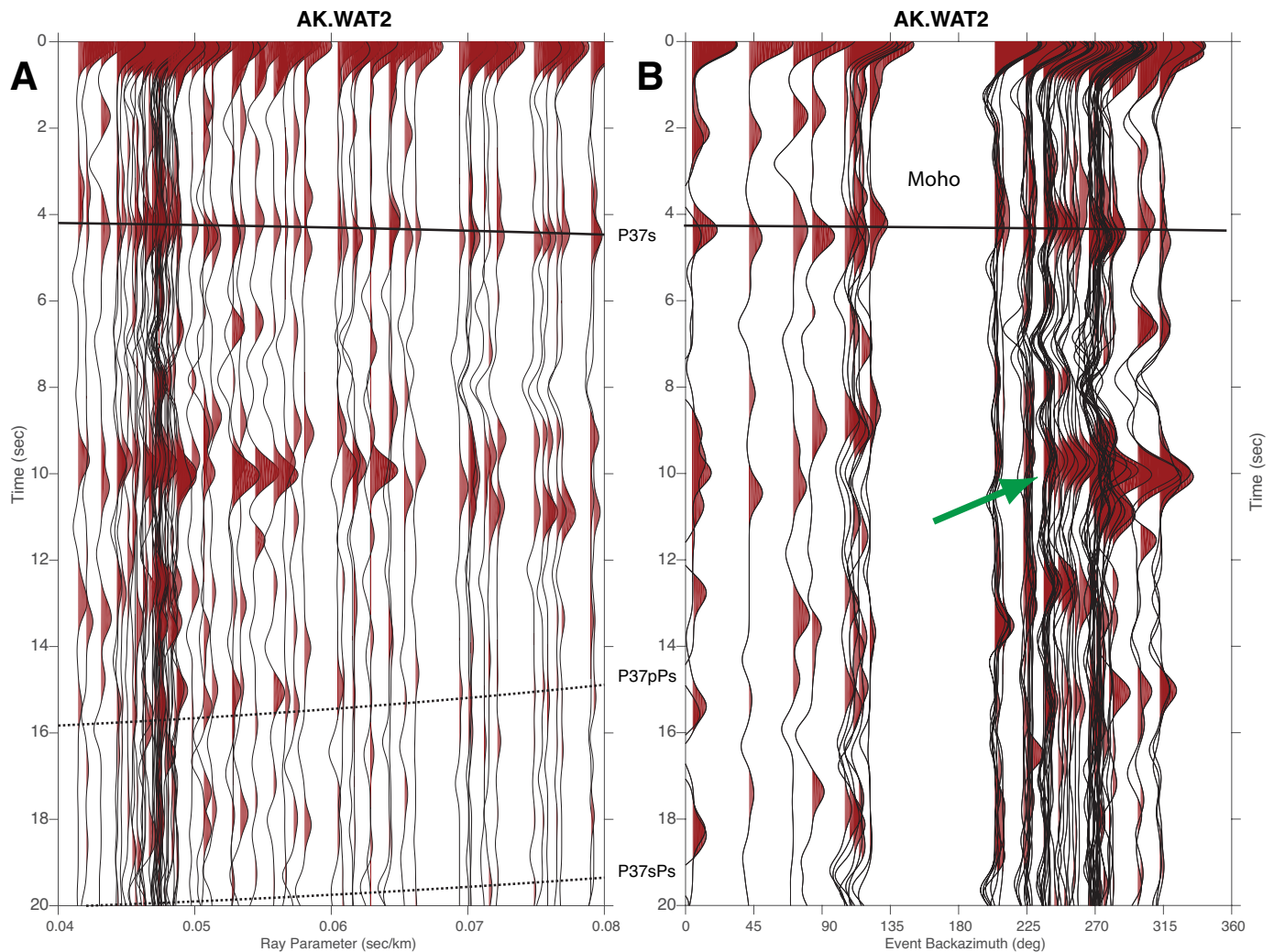


**Figure 6.** Receiver function record sections for station AK.WAT2. The location of the station is shown in Figures 1B and 5. (A) Record section sorted by ray parameter (moveout) with predicted arrivals for the Moho phase (P37s) and multiples (P37pPs and P37sPs) for a 37-km-deep Moho indicated by dashed lines. (B) Record section sorted by backazimuth with the Moho conversion indicated with a solid line; green arrow points to a large-amplitude positive conversion at ~10 s before the first crustal multiple.

boundary of thicker crust in the Yukon-Koyukuk basin and Brooks Range with thinner crust in the Ruby terrane fits with a proposed strike-slip model for escape of the Ruby terrane from the southern Brooks Range prior to the crustal-scale duplexing in the latter (Roeske et al., 2000; Till et al., 2014; Till, 2016; Roeske et al., 2017). In this model, the southern Brooks Range and the Ruby terrane share a common age and origin as a Paleozoic continental margin subducted beneath an arc in the Jurassic, but they separated in the Early Cretaceous. The preservation of varying crustal thicknesses between these three tectonically distinct terranes strongly suggests that the current crustal thickness in this region has been little modified since the late Mesozoic.

The uplands and lowlands south of the Tintina fault and north of the Denali fault contain a number of poorly exposed continental margin assemblages, variably metamorphosed, as well as arc basement rocks, remnants of closed ocean basins, and rare ultramafic and eclogitic rocks. One of the largest of these composite units is the YTT, which includes parautochthonous North America margin interpreted to be underthrust beneath thinned continental crust with Permian arc assemblages (e.g.,

Hansen and Dusel-Bacon, 1998). This collisional system was highly modified in the Mesozoic, probably with Jurassic shortening and Cretaceous extension (Hansen and Dusel-Bacon, 1998; Pavlis et al., 1993; Nelson et al., 2006). The current crustal thickness within the YTT has been inferred to be the result of the Cretaceous extension (cf. Beaudoin et al., 1994; Eberhart-Phillips et al., 2006; Brennan et al., 2011).

### Denali Fault and the Alaska Range

The central and eastern Alaska Range has been a focus of previous studies, but new TA data included with those from temporary arrays provide a new view on the region in a wider context. At the large scale, Figure 2A illustrates the significant topography in the Moho from south to north, and highlights the presence of steps across faults that have been previously identified as terrane boundaries. There is a significant change in Moho depth across the northern flank of the Alaska Range. The Alaska Range crust is thicker (~32–42 km) than that of the low topography block to the north (~27 km), as shown by the Moho depth map (Figs. 4 and 5). The

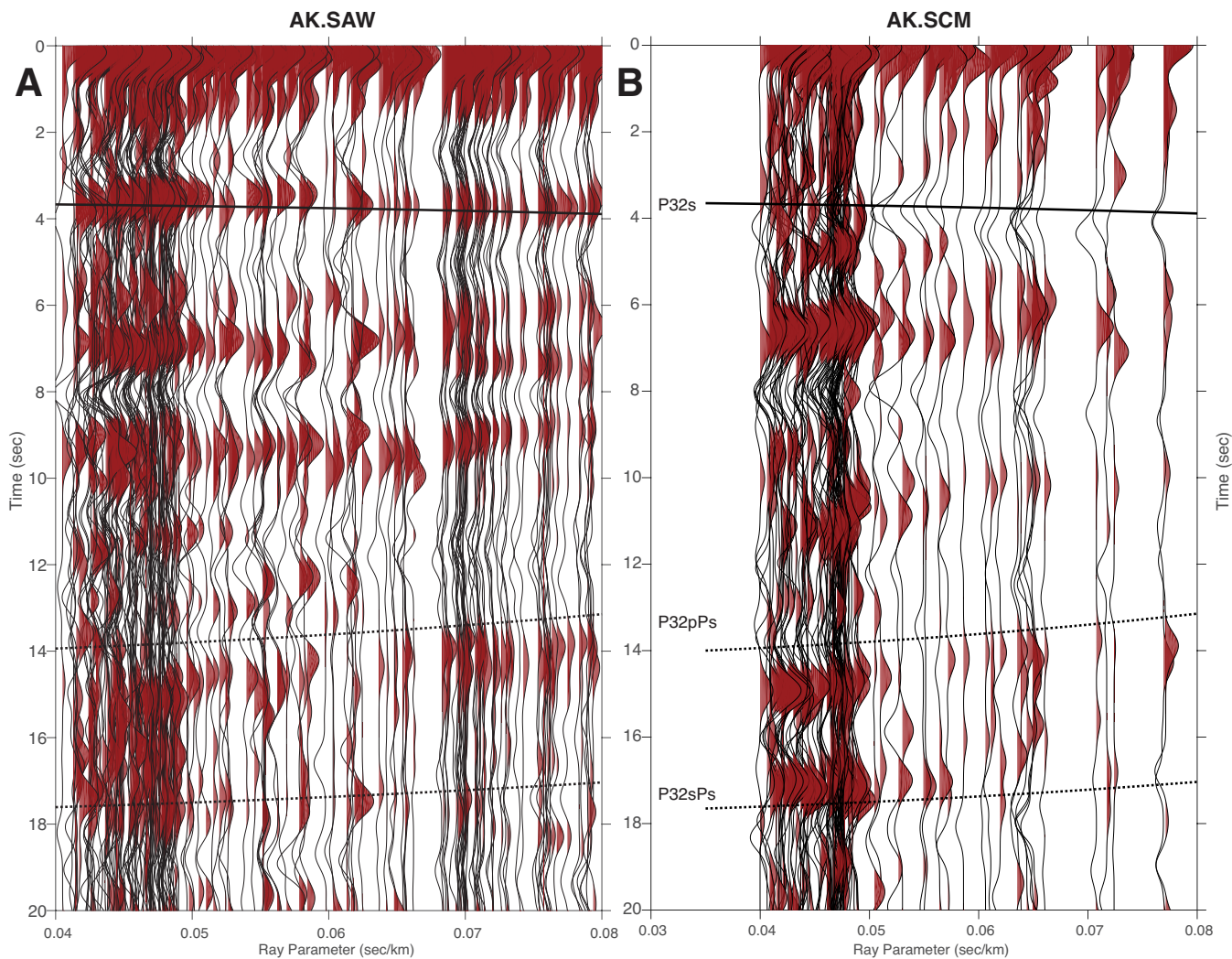


**Figure 7.** Receiver function record sections sorted by ray parameter (moveout) with predicted arrivals for the Moho phase (P32s) and multiples (P32pPs and P32sPs) for a 32-km-deep Moho indicated, respectively, by the solid and dashed lines. The locations of the stations are shown in Figures 1B and 5. (A) Station AK.SAW, Chugach Range. (B) Station AK.SCM, Chugach Range.

seismically active Denali fault includes a section through the suture zone between the YTT and WCT (Fig. 5) (Ridgway et al., 2002), and it is interesting that this part does not show significant offset in the Moho. Instead, a sharp step (~9 km) occurs across the Hines Creek fault, a terrane-bounding fault on the north side of the suture zone. The localized change in crustal thickness is also clearly depicted in the receiver function stacks (Figs. 3B, 3C). Similar results have been observed by other receiver function analyses, predicted calculations from Airy isostasy, and tomographic images of this region (Veenstra et al., 2006; Brennan et al., 2011; Allam et al., 2017). Allam et al. (2017) imaged a velocity contrast across the fault with a ~1 km resolution, which was then used to infer a ~10 km nearly vertical step with depth-converted PRFs. This estimate agrees with the magnitude of the step imaged here (~9 km) despite using the whole mantle 3D velocity model GyPSuM (Simmons et al., 2010) for the depth migration.

The Moho step across the Hines Creek fault is at least in part an inherited feature from Mesozoic collision of WCT with North America, but the Miocene to present geologic history of convergence and active thrust seismicity across this boundary suggests that the high-angle boundary is being modified by oblique convergence (Veenstra et al., 2006; Brennan

et al., 2011). East of the juncture between the Hines Creek and Denali faults, where the suture zone composite crust has been truncated, the abrupt change in Moho depth across the Denali fault records the strike-slip juxtaposition of the thinned continental crust of the Yukon-Tanana terrane from Wrangellia (Fuis et al., 2008).

Two aspects of the Alaska Range suture zone cross sections are intriguing and help address unsolved questions. First, why does the active trace of the Denali fault depart from the Mesozoic terrane boundary between the YTT and Wrangellia and bisect the suture zone, rather than following the Hines Creek fault? This question has been discussed by many, and summarized by Haeussler (2008). St. Amand (1957) was the first to suggest that the small circle geometry of the active fault is in response to development of a block between the Denali fault and the subduction zone, rotating about a possible Euler pole in the Gulf of Alaska. The suture zone rocks are speculated to be weaker than the YTT; this would favor the current geometry (Fitzgerald et al., 2014). The lack of a step in the Moho across the portion of the Denali fault that is within the Alaska Range suture zone is a related problem. The fault is currently the most active intraplate strike-slip fault in the northern Cordillera, with current slip rates estimated from ~7.5 to 13 mm/yr in the

central to eastern Alaska Range (Matmon et al., 2006; Haeussler et al., 2017). An M7.9 earthquake in 2002 ruptured initially as a thrust focal mechanism on a splay thrust fault, but propagated on the Denali fault with almost pure strike-slip motion (Eberhart-Phillips et al., 2003). Rheologic models of post-seismic deformation from global positioning system studies near the fault require a weak zone penetrating throughout the crust beneath the active trace (Freed et al., 2006; Johnson et al., 2009). Geologic and geochronologic studies immediately north and south of the fault indicate that the active strand has been in the same location from the surface to mid-crustal depths for at least 25 m.y. (Benowitz et al., 2013). Thus one would predict that 25 m.y. of strike-slip displacement along this boundary would juxtapose terranes of different thicknesses, as is observed to the east of the Hines Creek fault–Denali fault intersection (Fig. 4). It could be a coincidence that the Moho thickness does not change across the boundary along this section of the Denali fault and the fault could still penetrate through the entire crust.

### Yakutat Terrane

At the northwestern end of CCP profile B (Fig. 2B), the shallow positive signal from the Moho conversion is quite clear and so is a deeper negative conversion from what is interpreted as the base of the lithosphere (lithosphere–asthenosphere boundary, LAB), but there is also a lower amplitude positive signal beneath the negative amplitude LAB signal. We interpret this as the subducted Yakutat terrane. The signal from the Yakutat terrane is even more evident from analysis of individual station stacks and station gathers. This signal is particularly clear in the receiver functions at station AK.WAT2 (Fig. 6), which is located in the Alaska Range north of the Talkeetna fault (Figs. 1B and 5). The receiver gathers for this station (Fig. 6) along with the positive signal near the 300 km mark in the CCP profile shown in Figure 2B suggest that the positive signal at ~90 km depth is a conversion resulting from the leading edge of the subducted Yakutat terrane. This is in agreement with seismic tomography produced from the BEAAR array stations, east of AK.WAT2, used by Eberhart-Phillips et al. (2006) that identified a low-velocity zone atop of the subducting plate (as a positive conversion), and was interpreted as the subducting Yakutat first by Ferris et al. (2003), and then by Rondenay et al. (2008) at a similar depth range (~90 km).

In contrast, the southeastern end of CCP profiles B and C (Figs. 2B, 2C), which is nearly parallel to the coast through the inferred Yakutat terrane (Fig. 1), shows a deep (~65 km) positive signal. This would be extremely deep for the continental North American Moho. However, in the individual receiver function gathers and record sections, there are two separate positive pulses, not just one that is shown in the CCP profiles, that can be identified at several stations (AK.SAW, AK.SCM, AK.KLU; Figs. 3 and 6; Fig. DR1C) in the Chugach Mountains at the northern edge of the Wrangellia terrane (see Figs. 1B and 5 for station locations). The continental Moho appears at ~32 km and the Yakutat Moho is the deeper pulse (>55 km). Station AK.SAW is placed well within the Talkeetna arc, which is part of the WCT. Station AK.SCM is within a Cretaceous forearc basin, and thus may reflect that the crust beneath the forearc basement has been modified by subduction erosion. We suggest that the deep Moho observed is the base of the Yakutat as the microplate has subducted beneath the North American plate, similar to the interpretation of Worthington et al. (2012) and Bauer et al. (2014). Where there is not a strong velocity contrast, there is no conversion and where there are significant heterogeneities in the crustal structure, the fine-scale structure is smoothed out and obscured by the CCP imaging process.

### Wrangell Volcanic Field

The cross section in Figure 2B images a clear positive (red) shallow conversion at either end of the profile, but there is no signal in the center of

the profile. This portion of the profile is just south of the Wrangell Volcanic Field (Fig. 1B). However, there was no lack of Moho signal in S receiver function profiles through this region by O'Driscoll and Miller (2015) or by Bauer et al. (2014), which used similar, yet smaller data sets. However, when compared to the S receiver functions of O'Driscoll and Miller (2015) and plotted with the PRF hit count (Fig. DR2), the lack of signal may mostly be attributed to the lack of ray path coverage in this part of the image volume. This lack of signal and also lack of clearly interpreted structure has been an ongoing topic of research, but will likely be addressed by a new USArray Flex Array experiment (Christensen and Abers, 2016), which has deployed 27 broadband instruments in this area that previously had very few stations.

### Alaska Peninsula and Aleutian Range

The current sparse station density and variable data quality along the Alaska Peninsula and out to the Aleutian Islands provides a glimpse at the crustal structure in the region. Many of the high-quality stations appear to be located on relatively thick crust (Figs. 3K, 3L, and 4), but additional data are needed to interpret the more detailed structure along the arc. This will likely be addressed with more TA stations, but also by the SALMON (Southern Alaska Lithosphere and Mantle Observation Network) experiment (Tape et al., 2017), which has recently deployed 18 broadband stations across Cook Inlet and into the Alaska Range.

### CONCLUSIONS

Combining the three different receiver function methodologies, i.e., CCP stacking, individual receiver function stacks, and receiver gathers, for viewing and imaging PRFs allows for an interpretation of Alaskan crustal structure that spans multiple scales. We produce a Moho depth map in which we observe a primary trend that the crustal thickness roughly correlates with topography: (1) thick crust beneath the Brooks Range and northern Alaska; (2) thinner crust in the YTT in central Alaska; and (3) thick crust beneath the Alaska Range. We also find that the Moho depths at more remote stations that cannot effectively be included in the CCP volume are able to be interpreted individually and provide new valuable information on the geometry of various terrane boundaries and highlight the importance of this more detailed examination that avoids the smoothing associated with CCP analysis. There are striking changes in crustal thickness at these boundaries, and our detailed look at individual receiver functions throughout Alaska shows variability that appears to reflect inherited thickness from Mesozoic transform, convergent, and extension events. In some regions the crust is being extensively modified by ongoing convergence and collision, particularly along the active southern margin, yet the crust can maintain its original thickness. With additional data from the newly installed USArray TA stations outside of south-central Alaska, the crustal and mantle lithospheric structure appears to be as equally complex as the best studied region, and as more data become available through EarthScope and other deployments, an even more detailed crustal structure picture will emerge. The addition of the 4D component will improve models of how lithosphere rheology can be modified along diffuse plate boundary zones.

### ACKNOWLEDGMENTS

All data used in this work were downloaded from the Incorporated Research Institutions for Seismology Data Management Center (IRIS-DMC); DOI citations are listed in Table DR1. Funding for this work was provided through National Science Foundation CAREER award EAR-1054638 to Miller. The updated version of FuncLab is available online (<http://robporritt.wordpress.com/software>) and implements processRFmatlab for calculation of receiver functions (<https://github.com/iwbailey/processRFmatlab>).

### REFERENCES CITED

Allam, A.A., Schulte-Pelkum, V., Ben-Zion, Y., Tape, C., Ruppert, N., and Ross, Z., 2017, Ten kilometer vertical Moho offset and shallow velocity contrast along the Denali fault from



- double-difference tomography, receiver functions, and fault zone head waves: *Tectonophysics*, v. 721, p. 56–69, <https://doi.org/10.1016/j.tecto.2017.09.003>.
- Bauer, M.A., Pavlis, G.L., and Landes, M., 2014, Subduction geometry of the Yakutat terrane, southeastern Alaska: *Geosphere*, v. 10, p. 1161–1176, <https://doi.org/10.1130/GES00852.1>.
- Beaudoin, B.C., Fuis, G.S., Lutter, W.J., Mooney, W.D., and Moore, T.E., 1994, Crustal velocity structure of the northern Yukon-Tanana upland, central Alaska: Results from TACT refraction/wide-angle reflection data: *Geological Society of America Bulletin*, v. 106, p. 981–1001, [https://doi.org/10.1130/0016-7606\(1994\)106<0981:CVSOTN>2.3.CO;2](https://doi.org/10.1130/0016-7606(1994)106<0981:CVSOTN>2.3.CO;2).
- Benowitz, J.A., Layer, P.W., and Vanlaningham, S., 2013, Persistent long-term (c. 24 Ma) exhumation in the eastern Alaska Range constrained by stacked thermochronology, *in* Jourdan, F. et al., eds., *Advances in <sup>40</sup>Ar/<sup>39</sup>Ar dating, from archeology to planetary sciences*: Geological Society of London Special Publication 378, p. 225–243, <http://dx.doi.org/10.1144/SP378.12>.
- Brennan, R.R., Gilbert, H., and Ridgway, K.D., 2011, Crustal structure across the central Alaska Range: Anatomy of a Mesozoic collisional zone: *Geochemistry, Geophysics, Geosystems*, v. 12, Q04010, <https://doi.org/10.1029/2011GC003519>.
- Christensen, D., and Abers, G., 2016, Fate and consequences of Yakutat terrane subduction beneath eastern Alaska and the Wrangell Volcanic Field: International Federation of Digital Seismograph Networks, Other/Seismic Network, [https://doi.org/10.7914/SN/YG\\_2016](https://doi.org/10.7914/SN/YG_2016).
- Christeson, G.L., Van Avendonk, H.J.A., Gulick, S.P.S., Reece, R.S., Pavlis, G.L., and Pavlis, T.L., 2013, Moho interface beneath Yakutat terrane, southern Alaska: *Journal of Geophysical Research*, v. 118, p. 5084–5097, <https://doi.org/10.1002/jgrb.50361>.
- Cross, R.S., and Freymueller, J.T., 2008, Evidence for and implications of a Bering plate based on geodetic measurements from the Aleutians and western Alaska: *Journal of Geophysical Research: Solid Earth*, v. 113, <https://doi.org/10.1029/2007JB005136>.
- Dueker, K.G., and Sheehan, A.F., 1997, Mantle discontinuity structure from midpoint stacks of converted P to S waves across the Yellowstone hotspot track: *Journal of Geophysical Research*, v. 102, p. 8313–8327, <https://doi.org/10.1029/96JB03857>.
- Eagar, K.C., and Fouch, M.J., 2012, FuncLab: A MATLAB interactive toolbox for handling receiver function datasets: *Seismological Research Letters*, v. 83, p. 596–603, <https://doi.org/10.1785/gssrl.83.3.596>.
- Eberhart-Phillips, D., et al., 2003, The 2002 Denali fault earthquake, Alaska: A large magnitude, slip partitioned event: *Science*, v. 300, p. 1113–1118, <https://doi.org/10.1126/science.1082703>.
- Eberhart-Phillips, D., Christensen, D.H., Brocher, T.M., Hansen, R., Ruppert, N.A., Haeussler, P.J., and Abers, G.A., 2006, Imaging the transition from Aleutian subduction to Yakutat collision in central Alaska, with local earthquakes and active source data: *Journal of Geophysical Research*, v. 111, B113003, <https://doi.org/10.1029/2005JB004240>.
- Ferris, A., Abers, G.A., Christensen, D.H., and Veenstra, E., 2003, High resolution image of the subducted Pacific (?) plate beneath central Alaska, 50–150 km depth: *Earth and Planetary Science Letters*, v. 214, p. 575–588, [https://doi.org/10.1016/S0012-821X\(03\)00403-5](https://doi.org/10.1016/S0012-821X(03)00403-5).
- Finzel, E.S., Trop, J.M., Ridgway, K.D., and Enkelmann, E., 2011, Upper plate proxies for flat-slab subduction processes in southern Alaska: *Earth and Planetary Science Letters*, v. 303, p. 348–360, <https://doi.org/10.1016/j.epsl.2011.01.014>.
- Fitzgerald, P.G., Roeske, S.M., Benowitz, J.A., Riccio, S.J., Perry, S.E., and Armstrong, P.A., 2014, Alternating asymmetric topography of the Alaska Range along the strike-slip Denali fault: Strain partitioning and lithospheric control across a terrane suture zone: *Tectonics*, v. 33, p. 1519–1533, <https://doi.org/10.1002/2013TC003432>.
- Freed, A.M., Bürgmann, R., Calais, E., Freymueller, J., and Hreinsdóttir, S., 2006, Implications of deformation following the 2002 Denali, Alaska, earthquake for postseismic relaxation processes and lithospheric rheology: *Journal of Geophysical Research*, v. 111, B01401, <https://doi.org/10.1029/2005JB003894>.
- Freymueller, J.T., Woodard, H., Cohen, S.C., Cross, R., Elliott, J., Larsen, C.F., Hreinsdóttir, S., and Zweck, C., 2013, Active deformation processes in Alaska, based on 15 years of GPS measurements, *in* Freymueller, J.T., et al., eds., *Active tectonics and seismic potential of Alaska*: American Geophysical Union Geophysical Monograph 179, p. 1–42, <https://doi.org/10.1029/179GM02>.
- Fuis, G.S., et al., 2008, Trans-Alaska Crustal Transect and continental evolution involving subduction underplating and synchronous foreland thrusting: *Geology*, v. 36, p. 267–270, <https://doi.org/10.1130/G24257A.1>.
- Haeussler, P.J., 2008, An overview of the neotectonics of interior Alaska: Far-field deformation from the Yakutat microplate collision, *in* Freymueller, J.T., et al., eds., *Active Tectonics and Seismic Potential of Alaska*: American Geophysical Union Geophysical Monograph 179, p. 83–108, <https://doi.org/10.1029/179GM05>.
- Haeussler, P.J., Matmon, A., Schwartz, D.P., and Seitz, G.G., 2017, Neotectonics of interior Alaska and the late Quaternary slip rate along the Denali fault system: *Geosphere*, v. 13, p. 1–19, <https://doi.org/10.1130/GES01447.1>.
- Johnson, K.M., Bürgmann, R., and Freymueller, J.T., 2009, Coupled afterslip and viscoelastic flow following the 2002 Denali fault, Alaska earthquake: *Geophysical Journal International*, v. 176, p. 670–682, <https://doi.org/10.1111/j.1365-246X.2008.04029.x>.
- Kennett, B.L.N., Engdahl, E.R., and Buland, R., 1995, Constraints on seismic velocities in the Earth from travel times: *Geophys. J. Int.*, v. 122, p. 108–124.
- Kim, Y., Abers, G.A., Li, J., Christensen, D., Calkins, J., and Rondenay, S., 2014, Alaska megathrust 2: Imaging the megathrust zone and Yakutat/Pacific plate interface in the Alaska subduction zone: *Journal of Geophysical Research*, v. 119, <https://doi.org/10.1002/2013JB010581>.
- Ligorria, J.P., and Ammon, C.J., 1999, Iterative deconvolution and receiver-function estimation: *Bulletin of the Seismological Society of America*, v. 89, p. 1395–1400.
- Matmon, A., Schwartz, D.P., Haeussler, P.J., Finkel, R., Lienkaemper, J.J., Stenner, H.D., and Dawson, T.E., 2006, Denali fault slip rates and Holocene–late Pleistocene kinematics of central Alaska: *Geology*, v. 34, p. 645–648, <https://doi.org/10.1130/G22361.1>.
- McNamara, D. E., and M. E. Pasyanos, 2002, Seismological evidence for a sub-volcanic arc mantle wedge beneath the Denali volcanic gap, Alaska: *Geophys. Res. Lett.*, v. 29, <https://doi.org/10.1029/2001GL014088>.
- Nelson, J.L., Colpron, M., Piercey, S.J., Dusel-Bacon, C., Murphy, D.C., and Roots, C.F., 2006, Paleozoic tectonic and metallogenic evolution of the pericratonic terranes in Yukon, northern British Columbia and eastern Alaska, *in* Colpron, M., and Nelson, J.L., eds., *Paleozoic evolution and metallogeny of pericratonic terranes of the ancient Pacific margin of North America, Canadian and Alaskan Cordillera*: Geological Association of Canada Special Paper 45, p. 323–360.
- O'Driscoll, L.J., and Miller, M.S., 2015, Lithospheric discontinuity structure in Alaska, thickness variations determined by Sp receiver functions: *Tectonics*, v. 34, p. 694–714, <https://doi.org/10.1002/2014TC003669>.
- Pavlis, T.L., Sisson, V.B., Foster, H.L., Nokleberg, W.J., and Plafker, G., 1993, Mid-Cretaceous extensional tectonics of the Yukon-Tanana Terrane, Trans-Alaska Crustal Transect (TACT), east-central Alaska: *Tectonics*, v. 12, p. 103–122, <https://doi.org/10.1029/92TC00860>.
- Pavlis, T.L., Chapman, J.B., Bruhn, R.L., Ridgway, K., Worthington, L.L., Gulick, S.P., and Spottila, J., 2012, Structure of the actively deforming fold-thrust belt of the St. Elias orogen with implications for glacial exhumation and three-dimensional tectonic processes: *Geosphere*, v. 8, p. 991–1019, <https://doi.org/10.1130/GES00753.1>.
- Patton, W.W., and Box, S.E., 1989, Tectonic setting of the Yukon-Koyukuk Basin and its borderlands, western Alaska: *Journal of Geophysical Research: Solid Earth*, v. 94, p. 15807–15820, <https://doi.org/10.1029/JB094iB11p15807>.
- Plafker, G., and Berg, H.C., eds., 1994, *The geology of Alaska: Boulder, Colorado, Geological Society of America, The Geology of North America*, v. G-1, <https://doi.org/10.1130/DNAG-GNA-G1>.
- Porritt, R.W., and Miller, M.S., 2018, Updates to Funclab, a Matlab based GUI for handling receiver functions: *Computers & Geosciences*, v. 111, p. 260–271, <https://doi.org/10.1016/j.cageo.2017.11.022>.
- Ridgway, K.D., Trop, J.M., Nokleberg, W.J., Davidson, C.M., and Eastham, K.R., 2002, Mesozoic and Cenozoic tectonics of the eastern and central Alaska Range: Progressive basin development and deformation in a suture zone: *Geological Society of America Bulletin*, v. 114, p. 1480–1504, [https://doi.org/10.1130/0016-7606\(2002\)114<1480:MACTOT>2.0.CO;2](https://doi.org/10.1130/0016-7606(2002)114<1480:MACTOT>2.0.CO;2).
- Roeske, S.M., McClelland, W.C., and Snee, L.W., 2000, Extrusion of the Ruby terrane from the Brooks Range, Alaska, during early Cretaceous right-lateral strike-slip: *Geological Society of America Abstracts with Programs*, v. 32, no. 6, p. A-64.
- Roeske, S.M., Till, A.B., Miller, M.S., Saltus, R.W., and McClelland, W.C., 2017, Large vertical offsets of moho coincide with major mesozoic transform faults in northern Alaska: *Geological Society of America Abstracts with Programs*, v. 49, no. 6, doi: 10.1130/abs/2017AM-305345.
- Rondenay, S., Abers, G.A., and van Keken, P.E., 2008, Seismic imaging of subduction zone metamorphism: *Geology*, v. 36, p. 275–278, <https://doi.org/10.1130/G24112A.1>.
- Rondenay, S., Montési, L.G., and Abers, G.A., 2010, New geophysical insight into the origin of the Denali volcanic gap: *Geophysical Journal International*, v. 182, p. 613–630, <https://doi.org/10.1111/j.1365-246X.2010.04659.x>.
- St. Amand, P.S., 1957, Geological and geophysical synthesis of the tectonics of portions of British Columbia, the Yukon territory, and Alaska: *Geological Society of America Bulletin*, v. 68, p. 1343–1370, [https://doi.org/10.1130/0016-7606\(1957\)68\[1343:GAGSOT\]2.0.CO;2](https://doi.org/10.1130/0016-7606(1957)68[1343:GAGSOT]2.0.CO;2).
- Saltus, R.W., and Hudson, T.L., 2007, Regional magnetic anomalies, crustal strength, and the location of the northern Cordilleran fold-and-thrust belt: *Geology*, v. 35, p. 567–570, <https://doi.org/10.1130/G23470A.1>.
- Simmons, N.A., Forte, A.M., Boschi, L., and Grand, S.P., 2010, GPySuM: A joint tomographic model of mantle density and seismic wave speeds: *Journal of Geophysical Research*, v. 115, B12310, <https://doi.org/10.1029/2010JB007631>.
- Tape, C., Christensen, D., Moore-Driskell, M.M., Sweet, J., and Smith, K., 2017, Southern Alaska Lithosphere and Mantle Observation Network (SALMON): A seismic experiment covering the active arc by road, boat, plane, and helicopter: *Seismological Research Letters*, v. 88, p. 1185–1202, <https://doi.org/10.1785/0220160229>.
- Till, A.B., 2016, A synthesis of Jurassic and Early Cretaceous crustal evolution along the southern margin of the Arctic Alaska–Chukotka microplate and implications for defining tectonic boundaries active during opening of Arctic Ocean basins: *Lithosphere*, v. 8, p. 219–237, <https://doi.org/10.1130/L471.1>.
- Till, A.B., Roeske, S., Dumoulin, J.A., 2014, Escape of the Ruby terrane from Arctic Alaska during Mesozoic rotational opening of Canada basin: *Geological Society of America Abstracts with Programs*, v. 47, Paper 326-2.
- Trabant, C., Hutko, A.R., Bahavar, M., Karstens, R., Ahern, T., and Aster, R., 2012, Data products at the IRIS DMC: Stepping stones for research and other applications: *Seismological Research Letters*, v. 83, p. 846–854, <https://doi.org/10.1785/0220120032>.
- Veenstra, E., Christensen, D.H., Abers, G.A., and Ferris, A., 2006, Crustal thickness variation in south-central Alaska: *Geology*, v. 34, p. 781–784.
- Wang, Y., and Tape, C., 2014, Seismic velocity structure and anisotropy of the Alaska subduction zone based on surface wave tomography: *Journal of Geophysical Research*, v. 119, p. 8845–8865, <https://doi.org/10.1002/2014JB011438>.
- Ward, K.M., 2015, Ambient noise tomography across the southern Alaskan Cordillera: *Geophysical Research Letters*, v. 42, p. 3218–3227, <https://doi.org/10.1002/2015GL063613>.
- Worthington, L.L., Van Avendonk, H.J.A., Gulick, S.P.S., Christeson, G.L., and Pavlis, T.L., 2012, Crustal structure of the Yakutat terrane and the evolution of subduction and collision in southern Alaska: *Journal of Geophysical Research*, v. 117, B01102, <https://doi.org/10.1029/2011JB008493>.

MANUSCRIPT RECEIVED 21 AUGUST 2017  
 REVISED MANUSCRIPT RECEIVED 5 NOVEMBER 2017  
 MANUSCRIPT ACCEPTED 3 JANUARY 2018